IEEE Access
Multidisciplinary | Rapid Review | Open Access Journal

Received May 12, 2020, accepted May 23, 2020, date of publication May 29, 2020, date of current version June 10, 2020.

Digital Object Identifier 10.1109/ACCESS.2020.2998448

A Theoretical and Experimental Investigation on the Measurement of the Electromagnetic Field Level Radiated by 5G Base Stations

SARA ADDA[1], TOMMASO AURELI[2], STEFANO D'ELIA[3], DANIELE FRANCI[2], ENRICO GRILLO[2], MARCO DONALD MIGLIORE[4,5], (Senior Member, IEEE), SETTIMIO PAVONCELLO[2], FULVIO SCHETTINO[4], AND RICCARDO SUMAN[3]

[1]Dipartimento Rischi Fisici e Tecnologici, Arpa Piemonte, 10015 Ivrea, Italy
[2]Agenzia per la Protezione Ambientale del Lazio (ARPA Lazio), 00172 Rome, Italy
[3]Group Network, Vodafone Italia S.p.A, 10015 Ivrea, Italy
[4]Dipartimento di Ingegeria Elettrica e dell'Informazione (DIEI) "Maurizio Scarano", University of Cassino and Southern Lazio, 03043 Cassino, Italy
[5]ELEDIA@UniCAS Research Laboratory, Eledia Research Center, University of Cassino and Southern Lazio, 03043 Cassino, Italy

Corresponding author: Marco Donald Migliore (mdmiglio@ unicas.it)

This work was supported in part by the Italian Ministry of University and Research grant "Dipartimenti di Eccellenza 2018–2022".

ABSTRACT This paper presents some theoretical considerations and experimental results regarding the problem of maximum power extrapolation for the assessment of the exposure to electromagnetic fields radiated by 5G base stations. In particular the results of an extensive experimental campaign using an extrapolation procedure recently proposed for 5G signal is discussed and experimentally checked on a SU-MIMO signal. The results confirm the effectiveness of the extrapolation technique. Starting from an analysis (that represents a further novel contribution of this paper) on the impact of Spatial Division Multiple Access techniques used in 5G on the measurement of EMF level, some indications of possible extension of the technique to the highly complex MU-MIMO case are also given.

INDEX TERMS 5G mobile communication, antennas, base stations, health and safety, MIMO.

I. INTRODUCTION

Development of 5G has represented a huge engineering challenge. New technical solutions based on sophisticated strategies able to share the resources available in the communication channel among the users with unprecedented efficiency have been conceived and implemented, and, after a path full of difficulties, nowadays technology is mature for the deployment of the 5G. However, the implementation of this new technology is causing also an increasing concern about the possible impact on health and safety arising from exposure to radiofrequency (RF) electromagnetic radiation arising from 5G. To respond to this request of safety, two main problems need to be addressed. On one hand the study of the interactions between biological systems and Electromagnetic Fields (EMFs) is object of large research, whose results are condensed in the guidelines published by ICNIRP for the protection of humans exposed to radiofrequency electromagnetic fields. Such guidelines, that are at the basis of the national guidelines, include 5G, and are continuously updated with the latest scientific results [1]. On the other hand, effective techniques to measure the EMF level are required in order to check the compliance with the limits for 5G systems. Standards for 5G EMF measurement are under development by the International Electromechanical Commission (IEC) [2], [3]. However, due to the novelty and complexity of 5G technology, a limited number of results on this topic is available in the open scientific literature [4]–[7].

This paper represents a further contribution in the topic of measurement techniques for assessing RF EMF exposure in 5G communication systems.

One of the main problems in assessment of EMF exposure is related to the variation of the field level since radiated power of modern cellular communication systems changes over time with data traffic variation. In order to solve this problem, in the past generation of cellular systems maximum power extrapolation techniques have been proposed and successfully applied. Loosely speaking, these techniques allow

The associate editor coordinating the review of this manuscript and approving it for publication was Chinmoy Saha.

the estimation of the maximum level of the electromagnetic field that a base station can radiate in a given observation position from measurements taken in a relatively short temporal slot and represent a fundamental tool for assessing RF EMF exposure. The goal of this paper is a theoretical and experimental investigation of the maximum power extrapolation technique for 5G signals recently proposed by some of the authors of this paper [8], [9].

In Section II some characteristics of 5G technology relevant for EMF measurement are discussed. In particular, at the best knowledge of the authors, for the first time an analysis of the 5G signal at the lowest physical level, i.e. at the level of the electromagnetic field configuration, is carried out. The mathematical details of the method adopted to relate the concept of antenna ports to the electromagnetic field configuration are described in Appendix A.

Section III discusses the main point of the extrapolation method proposed in [8] and [9].

Section IV shows some results of a large experimental campaign regarding the application of the method proposed in [9] for the measurement of EMF level radiated by a 5G base station. More details about the method are given in Appendix B.

Section V discusses the limitation of the technique, suggesting some possible solutions.

Finally, in Section VI conclusions and indications for future work are discussed.

II. THE USE OF SPACE-TIME RESOURCES IN 5G COMMUNICATION SYSTEMS

One of the characteristics making the measurement of the electromagnetic field level of 5G signals so difficult is the unprecedented complexity of the space-time field configuration radiated by 5G antennas. This is a direct consequence of the unprecedented level of efficiency in the use of the space-time resources made available by the communication channel.

In this Section we will not enter into the details of 5G signals. A detailed description can be found, besides the 3GPP group reports and standards [10], in many excellent books on 5G, as for example [11], [12]. Instead, this Section will be focused on the understanding of some aspects of 5G signal relevant for the measurement of the electromagnetic field level.

A. THE USE OF THE RESOURCES IN THE TIME-FREQUENCY DOMAIN

NR supports two bandwidths: Frequency Range 1 (FR1), commonly referred to as sub-6 GHz, ranging from 450 MHz to 7.125 GHz, and Frequency Range 2 (FR2), commonly referred to as millimeter wave, ranging from 24.250 GHz up to 52.600 GHz. 5G NR uses Orthogonal Frequency-Division Multiple Access (OFDMA) and Cyclic Prefix with variable subcarrier spacing and OFDM-symbol duration. A NR carrier is made of up to 3300 subcarriers. The maximum bandwidth of each NR carrier is 100 MHz for sub-6 GHz band (FR1) and 400 MHz for millimeter band (FR2) [13]. NR allows to configure up to four bandwidth parts (BWP), wherein a bandwidth part is a subset of contiguous subcarriers. This allows to choose different bandwidths according to the request of the User Equipment (UE).

The time length of the NR frame is 10 ms and consists of 10 subframes, with a time length of 1 ms each [12], [13]. 5G NR uses a ''flexible numerology'' characterized by the parameter μ. Each NR subframe contains 2^{μ} slots, where μ can be 0, 1, 2, 3 or 4 [12], [13]. Each slot period (having $1/2^{\mu}$ ms time duration) contains 14 OFDM symbols (12 OFDM symbols in case of extended cyclic prefix). Consequently, the symbol duration is reduced according to the numerology [12]. Different numerologies are associated to different OFDM subcarrier distances. In particular, the subcarrier spacing turns out to be $2^{\mu} \cdot 15$ KHz. At ''data'' level, the smallest physical resource is represented by 1 subcarrier and 1 OFDM symbol and defines a ''Resource Element'' (RE). 12 consecutive subcarriers in the frequency domain constitute a Resource Block (RB), while the RBs and OFMD symbols in a subframe define a Resource Grid (RG).

B. SIGNALING STRUCTURE

NR has a sophisticated energy-efficient signaling structure, conceived to serve UE terminals having a wide range of different characteristics in terms of bandwidth, latency time and request of reliability. With reference to downlink transmission, on which this paper is focused, each physical channel (PDSCH, Physical Downlink Shared Channel, PDCCH, Physical Downlink Control Channel and PBCH, Physical Broadcast Channel) has its own Demodulation Reference Signal (DMRS) for channel estimation and equalization, that can be used as reference level for power allocation.

Furthermore, in order to obtain energy efficiency, NR has been conceived to avoid as much as possible ''always on'' signals. Consequently, in 5G there is only one ''always on'' NR signal, the Synchronization Signal/Physical Broadcast Channel (SS/PBCH), also called ''SS block'' (SSB), including the Synchronization Signals (SS), the PBCH and the PBCH-DMRS. The SS blocks are grouped in block patterns called SS bursts.

The structure of the SSB is very compact. SSB is mapped into 4 OFDM symbols in the time domain and 240 contiguous subcarriers (20 RBs) in the frequency domain. Furthermore, the signal is also concentrated in space since the SSBs are transmitted using directive beams (Fig. 1). Loosely speaking, SSBs are a directional version of synchronization signals that are transmitted with high periodicity.

C. THE USE OF THE RESOURCES IN THE SPACE DOMAIN

With reference to the space domain, 5G is able to use sophisticated SDMA (Space Division Multiple Access) techniques based on MIMO technology. The ability to transmit independent information using the same time/frequency resources is quantified in the concept of ''antenna port'', defined by 3GPP ''such that the channel over which a symbol on the antenna

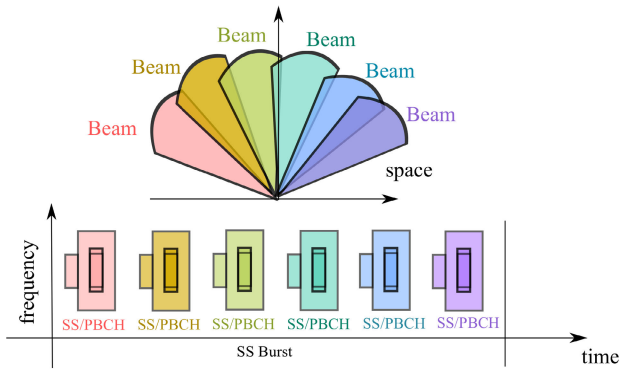

FIGURE 1. The figure shows the SSB in a SS Block (lower figure); each SSB is associated to a different antenna beam point; this strategy allows a fast covering of the entire sector of interest with signals highly concentrated in time and angular space.

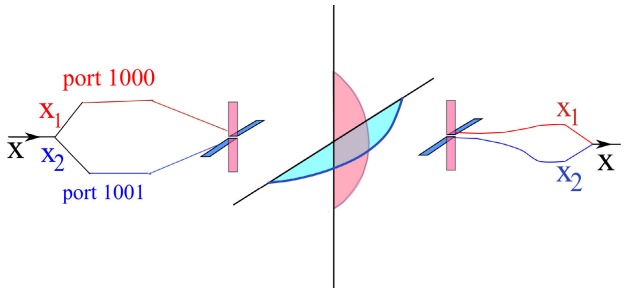

FIGURE 2. Idealized scheme of a polarization multiplexing MIMO communication system; the symbol x is divided into two parts, x_1 and x_2, that are transmitted using different polarizations and hence orthogonal field distributions (represented by the two orthogonal blue and red half-sinusoids); the receiving antennas are matched in polarization with the transmitting antennas, allowing to restore x [16].

port is conveyed can be inferred from the channel over which another symbol on the same antenna port is conveyed''. In practice, each antenna port is associated to a resource grid and a specific set of reference signals in the grid, allowing the reuse of the space-time resources of the channel. Different ranges of numbers are associated to ports used for different purposes.

It is worth noting that RG and antenna ports allow a huge flexibility in the 5G transmission. Indeed, the overall carrier bandwidth can be segmented in different resource grids, each being identified by direction of the transmission (Uplink or Downlink), numerology and antenna port.

RG and antenna ports are a powerful description of 5G signal structure at 'high level'. However, for our purpose a description of a lower 'physical level' is required.

In fact, while the mapping process between RG and time-bandwidth characteristics of the field radiated by the antenna is relatively straightforward, the mapping process between the antenna ports and the spatial configuration of the field is much less intuitive and, at the best knowledge of the authors, has never been investigated in details.

As previously noted, NR uses a wide range of SDMA techniques, from simple beam switching to sophisticated MU-MIMO (Multi-User Multiple Input Multiple Output) strategies [14]. Implementation of such techniques is completely at the will of the manufacturer. Furthermore, the NR signaling structure has been designed so that the system does not require the details of the beamforming, making the UE completely transparent to the physical details of the communication.

Analysis of communication at the basic physical level (i.e. at the level of electromagnetic field configuration) using standard approaches requires specific models for the many possible beamforming techniques that can be implemented in NR. In the following we use a unit approach for all the different techniques, including switched beam antennas, steering beam antennas, smart antennas, SU-MIMO and MU-MIMO, as well as diversity/multiplexing spatial communication. The method is briefly described in Appendix A, whereas for a deeper discussion the interested reader is invited to refer to [15] and [16].

In order to give a practical example, let us consider the PDSCH physical layer processing in case of a simple 2×2 MIMO communication as described in 5G specification [12]. After a number of steps, including channel coding and modulation, the code word is mapped onto 2 layers. Then, each layer is mapped to an antenna port, that, in case of PDSCH starts from number 1000 [12]. At the receiving side, the process is inverted obtaining the code word from the two antenna ports.

Now, let us consider the communication process at the lowest physical level.

First of all it is useful to note that MIMO transmission can be based on two different physical phenomena. Polarization multiplexing takes advantage of the vector nature of electromagnetic field. The transmission process is shown in Fig. 2. The code word x is divided into two parts that are transmitted on the two orthogonal polarizations. A polarization-matched receiving antenna receives the two signals allowing to restore x. In this model, each polarization is associated to a different port. It is understood that this is a simplified model, and in real communication channels cross-polarization arises from reflections. However, this requires only a linear processing of the signal, without any conceptual modification of the analysis.

Spatial multiplexing is a bit more involved and encodes information in the spatial distribution of the field. Loosely speaking, the code word x is divided into two sub-streams that are distributed to the radiating elements in a smart way by a proper beamforming network represented by a matrix $\mathbf{W}$. On the antenna surface we have a surface current density depending on x. The field radiated by the currents impinges on the user device, that measure the field in different points in the space using multiple antenna receiving elements. Measurement using multiple antennas placed in different positions of the space is equivalent to a spatial sampling of the electromagnetic field configuration. Since the field distribution in the space depends on the radiating currents, it is possible to retrieve the transmitted information.

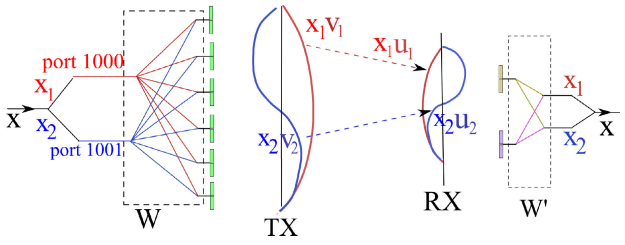

FIGURE 3. Idealized scheme of a spatial multiplexing MIMO communication system. From the left:the symbol x is divided into two subsymbols x_1 and x_2 and sent to the transmitting (TX) antennas through a proper beamforming network (matrix W); the current density distribution on the TX antennas is represented by the superposition of two current distributions v_1 and v_2, that give an incident field on the receiving (RX) antennas equal to u_1 and u_2 respectively; the amplitude and phase of the currents are modulated by x_1 and x_2. giving a global current density distribution on the TX antennas equal to $(x_1\ v_1 + x_2\ v_2)$; consequently, the field on the RX antennas is $(x_1\ u_1 + x_2\ u_2)$; a (spatial) sampling of the field using multiple RX antennas allows to retrieve x_1 and x_2 by a proper data processing (matrix W′), and hence x [16].

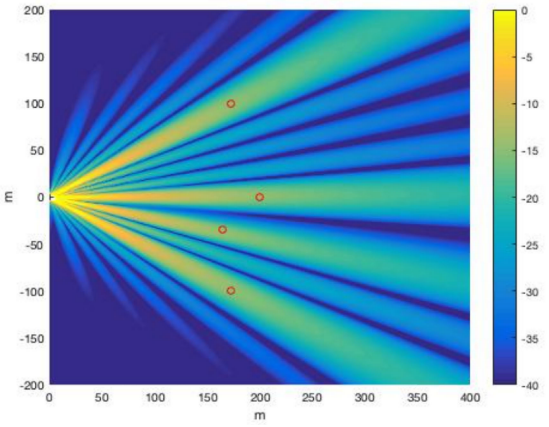

FIGURE 4. Example of the field distribution in MU-MIMO communications [$dB_{V/m}$] (free space propagation condition); the MU-MIMO antenna is on the left; the users are drawn as circles [18].

In order to explain the physical mechanism at the basis of multiplexing communication, let us represent the current distribution on the transmitting antenna and the incident field on the receiving antenna as a superposition of some special current basis, let v_k, $k = 1, \ldots, Q$, and field configuration basis let u_k, $k = 1, \ldots, Q$, chosen so that modification on the amplitude and/or phase of a current basis, let v_h be, causes the same variation of amplitude and/or phase on the associated field configuration basis u_h and only on u_h (see Appendix A). Each basis can convoy an independent piece of information with respect to the others, and hence each basis is the physical counterpart of a parallel spatial MIMO subchannel. Consequently, each port is associated to a different basis u_h and v_h. The number of layers and ports depends on how many u_h different basis functions are distinguishable in presence of noise, i.e. on the Number of Degrees of Freedom of the electromagnetic field at the *epsilon* level of accuracy (NDF_ϵ) [17].

It is understood that such parallel channels can be used (totally or partially) to send independent information, obtaining an improvement of the system throughput (MIMO multiplexing gain), or also to send statistically dependent information, obtaining an improvement of the reliability of the transmission (MIMO diversity gain), while the use of only the first basis function gives the so called ''MIMO beamforming'' [17].

It is also understood that the field configurations basis takes full advantage of the environment, and in presence of scattering clusters they generally give complex multiple-beams field configurations.

Now, we are in the right position to analyze the impact of ports in the measurement of the field level. In case of multiple layers, the field is given by the superposition of a number of electromagnetic field basis configurations whose amplitude and phase depend on the transmitted data. Even if the observation of the field at a single point of the space does not allow to distinguish the different basis, it gives a measure of the interference of such basis functions, that will change at the symbol rate according to the data associated to the different layers. Accordingly, it is possible to estimate the maximum of the field in a measurement position without decoding the layers provided that measurement time covers a sufficiently large number of transmitted symbols. However, it must be stressed that the measurement gives the value of the maximum amplitude of the field *in the measurement position*. The spatial distribution of the basis functions is quite complex [17]. Loosely speaking, the energy of the superposition of the basis functions (i.e. the incident field) tends to be concentrated toward the UEs (a more detailed analysis of the the relationship between information and energy is discussed in [15]). Consequently, in case of SU-MIMO (including also SISO (Single Input Sigle Output) systems), measurement of the field amplitude in the UE position allows an effective maximum power estimation. Instead, in MU-MIMO only a fraction of the energy is radiated toward a single UE, making the estimation of the maximum level of the EMF from measurement of the EMF maximum level in the UE positions a not straightforward task. In order to clarify this concept, in Fig. 4 an example of the field distribution in case of a MU-MIMO connecting 4 UEs is drawn. The figure clearly shows the distribution of available power among the users. As a consequence, in MU-MIMO antennas there is a reduction of the average EIRP (Effective Isotropic Radiated Power), i.e. of the maximum field level for a fixed total radiated power, compared to ''traditional'' systems, with a consequent reduction of the EMF level. Further details can be found in [18], whereas an interactive representation with moving users is available in [19].

Finally, at the level of the physical layer, no difference exists between the MIMO physical mechanisms. For example, the gNB used in the experimental campaign described in this paper takes full advantage of a mixture of polarization and space multiplexing to create up to 16 layers. These 16 layers could be independently assigned to one user

(SU-MIMO scenario) up to 8 users (MU-MIMO) were each user is using 2 layers. However, the difference plays a role in terms of measurement of the electromagnetic field level: in the SU-MIMO scenario if 2 or more users are active at the same time they are scheduled over time so that for a given RB only one user is served in a given instant of time. In the MU-MIMO scenario if 2 or more users are active at the same time they are scheduled simultaneously.

III. MAXIMUM POWER EXTRAPOLATION TECHNIQUE

As noted in the Introduction, the radiated power of 5G cellular communication systems varies with time depending on a number of factors including data traffic variation and position of the UEs. The goal of extrapolation techniques is the estimation of the maximum level of the electromagnetic field that a base station can radiate in a given observation position from measurements taken in a relatively short temporal slot.

Extrapolation techniques for cellular generations up to the 4^{th} one are based on well-defined procedures. The general approach is the identification of a proper component of the signal transmitted at constant power level, that is used as reference. For example, the BCCH (Broadcast Control Channel) signal is used in GSM base stations, the P-CPICH (Common Pilot Channel) is used in UMTS, whereas the Cell-specific Reference Signal (CRS) is adopted as reference signal in LTE. All these signals are always broadcast with constant and maximum power.

The approach followed in this paper for extrapolation of 5G signals has been developed in continuity with the procedure conceived for previous generations of cellular systems. The measurement procedure has been proposed in [8] and [9], where the reader can find a detailed description of the steps of the extrapolation process. In this Section the method is briefly summarized. A detailed description of the procedure proposed in [8] and [9] is reported also in Appendix B for sake of reader convenience.

As preliminary step, it is important to introduce the E_{5G}^{max} parameter. E_{5G}^{max} represents the maximum field level [V/m] that can be reached in the measurement point. From a practical point of view, it is representative of a 5G base station transmitting at its maximum power and concentrating all its power in a single beam (single user) during an extensive amount of time (e.g., 6 minutes is one of the averaging times required by the ICNIRP guidelines [1]). From a practical point of view, it can be reached only if the scheduler gives all the available resources to a single user continuously for at least 6 minutes, leaving all the other users in stand by (i.e. causing at least a 6 minutes loss of data connections to all the other subscribers of the cell). This quantity, referring to an unrealistic condition, is used as a reference to estimated the EMF exposure in realistic conditions by proper scaling factor, as discuss in Section V.

The maximum EMF level at a given location, E_{5G}^{max}, is estimated by the product of three factors

$$E_{5G}^{max} = \sqrt{N_{sc} F_{TDC}}\, E_{RE}^{max} \tag{1}$$

wherein

- N_{sc} is the total number of subcarriers of the NR carrier, i.e. twelve times the total number of Resource Blocks (N_{RB}) available for the signal;
- F_{TDC} is the deterministic scaling factor representing the duty cycle of the signal when TDD multiplexing strategy is used, i.e. the fraction of the signal frame reserved for downlink transmission;
- E_{RE}^{max} the maximum EMF level measured for a single Resource Element.

The procedures to evaluate F_{TDC} and N_{sc} are discussed in [8] and [9], and also reported in Appendix B. Regarding the evaluation of the third term, as discussed in the previous Section the only signal that is always 'on air' is the SSB. As previously noted, as a consequence of the beam sweeping, the received EMF level is different for each SSB, according to the relative orientation between the SSB beam and the receiver antenna (see Fig. 1).

In order to harmonize 4G and 5G extrapolation techniques, in [8] and [9] the PBCH Demodulation Reference Signal (PBCH-DMRS) is proposed as pilot channel. The PBCH-DMRS signal is one of the main parameters in NR and is directly measurable with great accuracy using modern Vector Spectrum Analyzers (VSAs) with demodulation software or also by network scanners.

In particular, E_{RE}^{max} can be obtained as:

$$E_{RE}^{max} = E_{RE,max}^{PBCH-DMRS} \sqrt{F_{beam}} \tag{2}$$

wherein:

- $E_{RE,max}^{PBCH-DMRS}$ is the maximum received EMF level for the PBCH-DMRS per RE;
- F_{beam} is a parameter which takes into account the effect of the boost of the traffic beams with respect to maximum EMF level received from the pilot channel, due to the effect of beamforming and beamsweeping.

With reference to $E_{RE,max}^{PBCH-DMRS}$, it can be evaluated from the maximum PBCH-DBRS power related to the strongest SSB and from the knowledge of the Antenna Factor (AF) of the antenna used in the field measurements and of the power losses α of the cable connecting the antenna and the measurement equipment using standard formulas,

$$E_{RE,max}^{PBCH-DMRS} = \sqrt{\frac{P_{RE,max}^{PBCH-DMRS} Z_{in}}{\alpha}} AF \tag{3}$$

wherein Z_{in} is the input impedance of the instrument. Some VSAs provide the detected PBCH-DMRS power for each SSB, allowing a direct evaluation of $P_{RE,max}^{PBCH-DMRS}$. If only an average over the SSBs is available, it can be related to $P_{RE,max}^{PBCH-DMRS}$ by

$$P_{RE,max}^{PBCH-DMRS} = \frac{< P_{RE}^{PBCH-DMRS} >}{R} \tag{4}$$

wherein R is defined as the ratio between the average detected power of all the SSBs in a burst and the power of the strongest

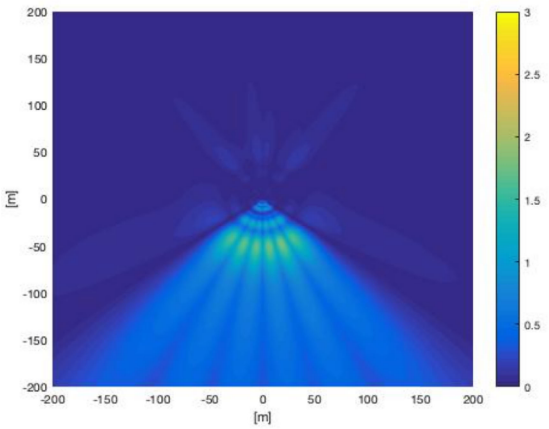

FIGURE 5. Example of the spatial distribution of the field [V/m] radiated by the beam-switched SSB signal antenna pattern (also called broadcast beam) during an SS Burst (free-space propagation condition, Massive MIMO 64T64R antenna).

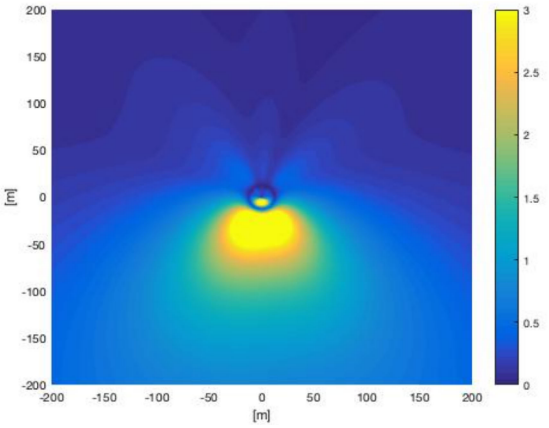

FIGURE 6. Example of the spatial distribution of the field [V/m] radiated by the beam-steering user data antenna pattern (also called traffic beam) (free-space propagation condition, Massive MIMO 64T64R antenna).

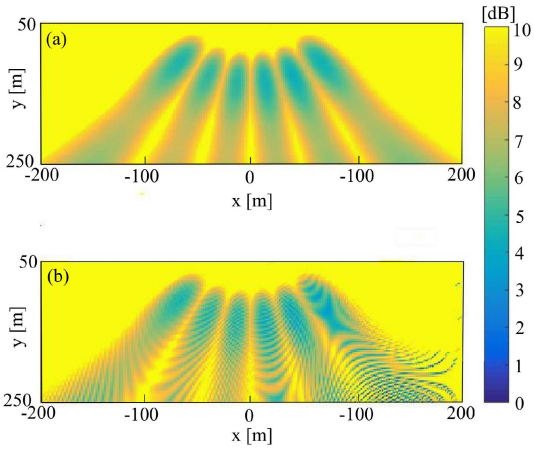

FIGURE 7. Ratio between the amplitude of the traffic beam and broadcast beam [dB]; (a) free space propagation; (b) in presence of a perfect electric conductor plane placed at x = 400 m.

SSB in the burst, and accounts for the effect of the beam sweeping on the received EMF level of all the SSBs in a burst.

Estimation of F_{beam} is the most critical procedure and requires a specific discussion.

F_{beam} is the ratio between the maximum power per RE of the PDSCHs and the maximum power per RE of the SSBs.

A possible way to estimate F_{beam} is by numerical simulations. 5G uses multi-beam and beam steering antennas, and the antenna characteristics are often given in terms of the so called 'envelope pattern', i.e. the envelope of the set of patterns that the beam-steering antenna can radiate. Consequently, F_{beam} can be estimated as the ratio between the field level radiated by the data pattern (i.e. the pattern carrying user data) and the signal pattern (i.e. the pattern carrying SSB data) in the measurement position. In spite of its apparent simplicity, this approach suffers from some drawbacks that cause large uncertainties. In order to clarify this point, in Fig. 5 the maximum field level received around an antenna carrying SSB signal is drawn according to the datasheet of the antenna used in the experimental campaign (a Massive MIMO 64T64R antenna), whereas in Fig. 6 the maximum field radiated for user data transmission is shown considering the same maximum transmitted power. The comparison of the level of the field in the two cases, showed in Fig. 7(a), confirms a strong variation of the ratio between the values of the fields with the position of the receiver. It must be stressed that the field distribution is valid in free space condition and does not consider the presence of the reflections and of scattering objects around the measurement point, that change the ratio. The ratio in case of a simple example regarding a planar reflecting surface placed 400 m far from the source is drawn in Fig. 7(b), showing a quite complex pattern. The accurate evaluation of F_{beam} has to take into account the reflection surfaces, including the soil, and can require complex simulations. The case of NLOS (Non Line of Sight) is much more complex. In fact while the SSBs are transmitted using a set of fixed-shaped beam patterns, the field configuration used for user-data transmission is environment-dependent and difficult to be predicted in case of radio links based on scattering objects, as discussed in Section II. Further problems arise in case of MIMO communications, for which antenna gain is not even rigorously defined. Furthermore, from a point of view of uncertainty evaluation, numerical estimation of the F_{beam} is affected by a number of factors, including a not complete knowledge of the environment (position, geometry and permittivity of the scattering objects) as well as approximations in the propagation model. Numerical simulations are as complex as the estimation of the field level itself, and are affected by a similar degree of accuracy. Finally, the use of F_{beam} value obtained by numerical simulations affects the final uncertainty of the estimated field level, giving a result whose level of confidence is of the same order of a direct estimation of the field level using computer simulations.

As a consequence, estimation of the F_{beam} from knowledge of the radiation pattern of the antennas is more complex and less effective than it could look like at a first glance.

In order to avoid the above recalled problems, in [9] an experimental procedure has been proposed to estimate F_{beam}. In particular the approach proposed in [9] requires to force the data beam toward the measurement position, and to measure the difference in dB between the highest SSB peak and the PDSCH associated to the UE placed at the measurement position level using a zero span measurement with a 1 MHz RBW centered on the SSBs center frequency. If PDSCH and SSBs share the same numerology, the ratio is equal to F_{beam}, otherwise a scaling factor must be taken into account.

For further details on the procedure, the reader is invited to refer to [9] and to Appendix B. The practical application of the procedure is also described in the next Section.

Before concluding this Section, some observations of the applicability of this technique in case of Massive MIMO are in order. Basically, Massive MIMO are antenna with a large number of elements. Consequently, from a 'physical' perspective the only difference compared 'standard' antennas is a vast enlargement of the set of the fields that can be radiated. This further flexibility opens new interesting possibilities from the point of view of the signal processing, but does bot change the general observations outlined for SU-MIMO and MU-MIMO in Section II. Consequently, the extrapolation method discussed in this paper can be applied also in case of gNB using Massive MIMO antennas in SU-MIMO configuration without any modification.

IV. EXPERIMENTAL VALIDATION

This Section describes the results obtained applying the extrapolation procedure described in the previous Section during a large measurement campaign. The discussion will be focused on 2 different test conditions, each analyzed in a specific Subsection. A further Subsection is devoted to the general description of the measurement site and instrumentation used in the measurement campaign.

A. MEASUREMENT SITE AND EQUIPMENT

The measurement site is shown in Fig. 8. The position of the 5G base station gNB is indicated with the label ''5G source''. The antenna is placed roughly at 20 m above the ground. The terminals are placed in the positions indicated as points A and B.

Data are acquired using a wide range of instrumentation, including:

1) a Keysight signal analyzer MXA N9020A connected to a Rohde & Schwarz Log-Periodic Antenna HL050;
2) a Rohde & Schwarz FSP30 spectrum analyzer connected to a Keysight N6850A Broadband Omnidirectional antenna;
3) a Rohde & Schwarz TSME network scanner, connected to a Rohde & Schwarz Qualipoc Android;
4) a Rohde & Schwarz FSW26 signal analyzer connected to a Rohde & Schwarz HE300 broadband antenna;
5) two 5G phones (Samsung Galaxy 10 5G) used to force the data traffic;

FIGURE 8. Measurement site; the measurement positions are labeled A and B; the 5G base station antenna is visible on the left.

TABLE 1. 5G signal configuration.

Center frequency [MHz]	3680.01
Bandwidth [MHz]	80
Duplexing	TDD
Time duty cycle factor F_{TDC}	0.743
Numerology (μ)	1
Symbol duration [μs]	33.3
CP duration [μs]	4.7
Symbols per slot	14
Slots per subframe	2
Slots per frame	20
Antenna	mMIMO 64T64R
Spatial Multiplexing	SU-MIMO
Number of layers used	4
SS Block center frequency [MHz]	3649.44
SS Burst configuration	C-case
Number of SSB per SS Burst	6

Note that the BS antenna supports up to 16 layer in downlink and 8 layers in uplink; in the measurement session the number of layers used in downlink was limited by the EUs to 4.

6) iPerf software (www.iperf.fr) used in UDP mode together with a server to control the downlink transmission.

The measurement instruments are placed at point A. The main characteristics of the signal transmitted by the base station, are reported in Table 1.

B. ANALYSIS OF THE SIGNAL IN ABSENCE OF DATA TRAFFIC

As preliminary step, measurements are carried out without any UE. These measurements allow to obtain a number of information about the parameters of the signal radiated by the base station. The spectrum of the received signal in no-data transmission condition is shown in Fig. 9. The spectrum allows to identify the bandwidth of the signal, equal to 80 MHz, as well as the frequency range used for SSB transmission. In fact, in absence of transmitted data the power spectral density is quite low in all the bandwidth range of the signal apart from the lower part of the bandwidth, where the power spectrum density significantly increases. This part of the bandwidth is used to transmit the SSB.

It is possible to observe the SS Block structure by using a zero span measurement mode and locking the frequency of spectrum analyzer at the central frequency of the high density power section of the band (3.65 GHz). As an example, figure 10 shows a zero span acquisition of the signal over

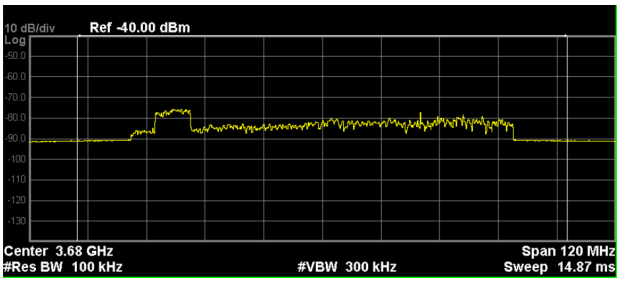

FIGURE 9. Spectrum of the received signal in no data transmission mode.

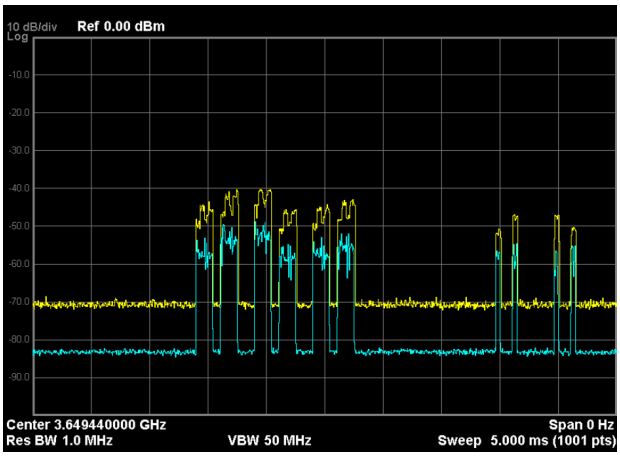

FIGURE 10. Zero span measurement of the signal in case of no data traffic (RBW = 1 MHz); yellow: max-hold trace; blue: average value.

a 10 ms sweep time using a 1 MHz RBW (Resolution Bandwidth). The yellow trace gives the maximum value in an observation interval of 10 s whereas the blue line gives the average value in the same time period.

The figure clearly shows the structure of the SS-Burst. The SS-Burst is composed by six SS Blocks configured according to "C" case [12]. From the time duration of a SSB ($4\tau \simeq 133\ \mu s$, wherein 4 is the number of symbols reserved for an SS-Block and τ represents the time of a symbol) it is possible to identify the numerology.

After the SSB, we can note also four spikes. These spikes are the hints of the presence of a sophisticated signaling structure.

A more detailed study can be performed by an analysis of the RE in a frame. As an example, Fig. 11 shows the power of the REs. The vertical axis covers the entire 80 MHz bandwidth. Regarding the horizontal axis, each segment between two consecutive vertical lines represents a slot (i.e. 500 μs, 14 OFDM symbols), whereas a subframe (1 ms) is given by 2 consecutive slots. Accordingly, the figure shows an entire frame (10 ms). The SS-Burst is visible in the lower left corner. The power of the REs associated to different SSBs changes according to the direction of the main beam of the signaling pattern. Even if barely distinguishable, it is possible to identify also a number of other non-zero power REs sparsely positioned in the grid, that are used for signaling. In particular,

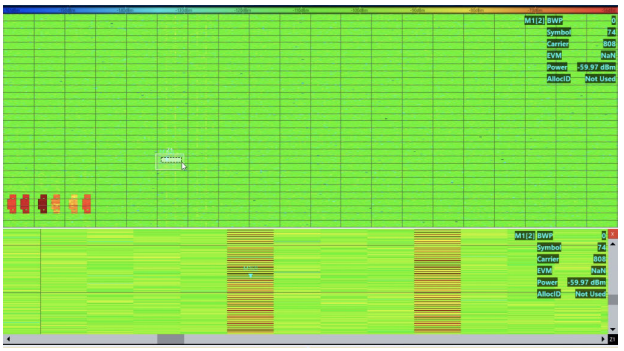

FIGURE 11. The figure shows the power per RE versus the subcarriers (vertical axis) and the OFDM symbols (horizontal axis) in a frame in case of no traffic data; the power is represented in false colors; the brightest red is −45 dBm; the upper part of the figure shows the entire RG; the lower part shows a zoom of the area of the grid indicated by the bright rectangle in the upper figure.

there are some signaling data in the 6^{th} and 7^{th} slots that are barely visible in the figure, but can be clearly distinguished when the image is zoomed (see lower part of Fig. 11, that is a zoomed section of the part limited by the brighter rectangle in the REs grid). Even if the average power per RE associated to the signaling is low, the REs span the entire band, giving a not negligible global power, and making the signals visible in the zero span measurements. This example shows that, apart from SSBs, there can be other signals in air also when no UE are present. However, the details of such signals are completely up to the manufacturer of the communication system, and their presence and characteristics are nor standardized neither predictable. Accordingly, their use for standardized field level measurements is questionable, and the only reliable 'always on air' signal that can be used as reference is the SSB.

C. ANALYSIS OF THE SIGNAL IN PRESENCE OF DATA TRAFFIC

In order to validate the extrapolation method we forced the base station antenna to transmit at the maximum power filling all the REs available for data transmission. For this purpose, two customized UE terminals able to force high-data download transmission using UDP (User Datagram Protocol) protocol are placed at A point, i.e. in the measurement point.

The maximum number of layers supported by the BS antenna is 16 in downlink and 8 in uplink. However, the UEs supported only 4 layers in uplink and 2 layers in downlink. Accordingly, during the measurements downlink communication supported 4 layers.

In Fig 12 the transmitted power (blue line) and the number of Resource Blocks (red line) during a measurement session are shown. The plot confirms the condition of complete use of the available resources during the measurement of the data showed in this Section.

In Fig. 13 a frame of the RE power grid in a case of full-use of the REs is shown in false color. The void regions (no RE power) in the 8/9/10/18/19/20 slots are reserved for uplink data. The control signals discussed in the previous

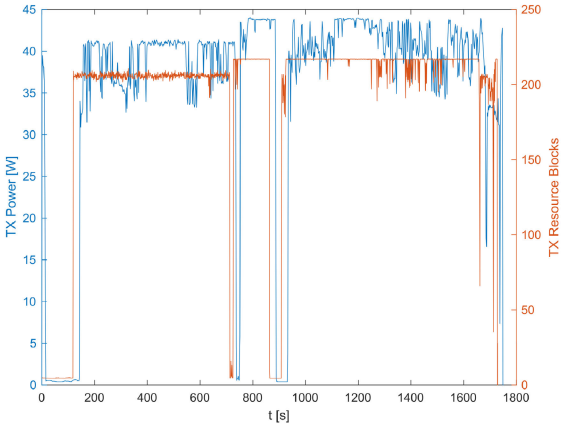

FIGURE 12. Trasmitted power level [dB] and number of transmitted Resource Blocks during a measurement session regarding the full data load examples showed in this paper.

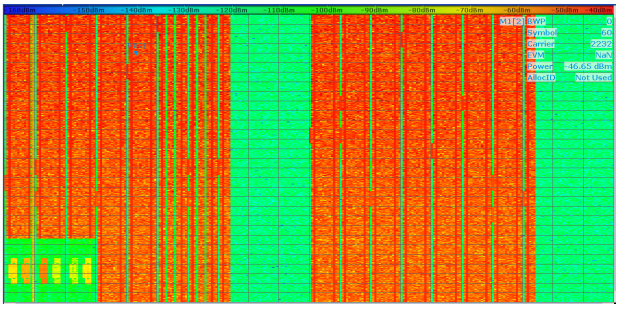

FIGURE 13. The power per RE versus the subcarriers (vertical axis) and the OFDM symbols (horizontal axis) in a frame in case of full use of the grid resources; the power level is plotted in false colors.

Subsections are also visible, ranging along all subcarriers in the slots 6 and 7. Many other control signals are placed in the Subcarrier-OFDM symbol grid. Among them, the PDSCH-DMRS are barely visible, in the OFDM symbol number 2 and number 11 of each slot, ranging for all the subcarriers used by the PDSCH. On the lower left side the typical structure of the SS Burst is clearly visible. Between the second and third SSB, signal data, with low average power but high peak power are transmitted along the whole frequency range.

The VSA with demodulation software is able to give directly the average power value of the PBCH-DMRS (Fig. 14(a)) and the power of the SSBs (Fig. 14(b). These data allow to estimate the maximum power level of PBCH-DMRS per RE, which turns out to be −69.88 dBm.

The next step is the evaluation of F_{beam}. We follow the procedure based on the measurement of the signals in zero span using peak detector described in [9]. With reference to Fig. 15, the SS Burst is visible on the left. The signaling data sent between the second and third SSB is clearly visible using max-hold trace function (yellow curve), while almost disappears using average trace function (blue curve). The value of F_{beam} is equal to 16.47 dB, giving an estimated maximum power per RE equal to −53.46 (Table 2).

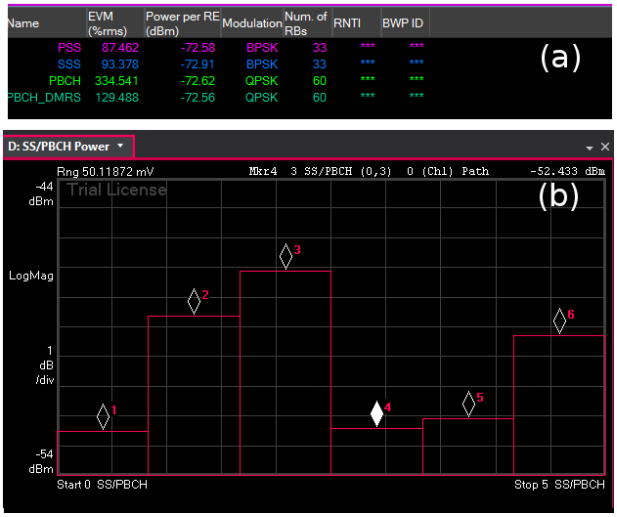

FIGURE 14. The figure shows a measure of the data required to estimate the maximum power per RE using the VSA; the upper part of the figure shows a list of parameters including the PBCH-DMRS; in the lower part the of the figure the power of the SSBs is shown.

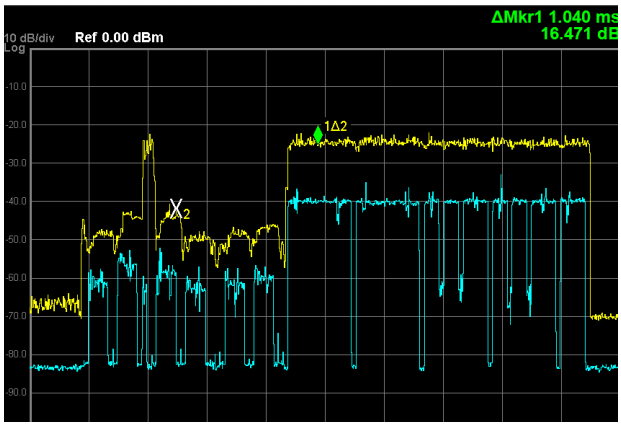

FIGURE 15. Zero span measurement of the signal in full-data conditions (1 MHz RBW); yellow: max-hold trace; blue: average value; the peak between the second SSB and the third SSB is a control signal.

Finally, the field amplitude is evaluated taking into account the attenuation of the cable connecting the antenna to the measurement device and the Antenna Factor (−5.09 dB and 32.61 dBi respectively), obtaining 1.87 V/m in case of full use of the resources, including the use of the RE reserved for upload connection. Finally, considering the F_{TDC} factor we obtain $E_{5G}^{max} = 1.61$ V/m.

In order to validate the result, Channel Power measurement is carried out using a Keysight signal analyzer MXA N9020A (fig. 16) and a Rohde & Schwarz FSP30 spectrum analyzer. The results are summarized in Table 3, wherein the values of the uncertainty at 95% percentile are also indicated. The Table confirm that the extrapolation value is within the range of uncertainty of the value estimated by Channel Power measurement.

TABLE 2. Measured data.

$< P_{RE}^{PBCH-DMRS} >$ [dBm]	-72.56
R	0.54
$P_{RE,max}^{PBCH-DMRS}$ [dBm]	-69.88
F_{beam} [dB]	16.47
E_{RE}^{max} [V/m]	1.87
E_{5G}^{max} [V/m]	1.61

TABLE 3. Field amplitude measured in A.

Method	Value	Uncertainty 95^{th} percentile
Extrapolation	1.61 V/m	$\pm$0.58 V/m
CP - Keysight MXA N9020A	1.72 V/m	$\pm$0.29 V/m
CP- Rohde & Schwarz FSP30	1.89 V/m	$\pm$0.45 V/m

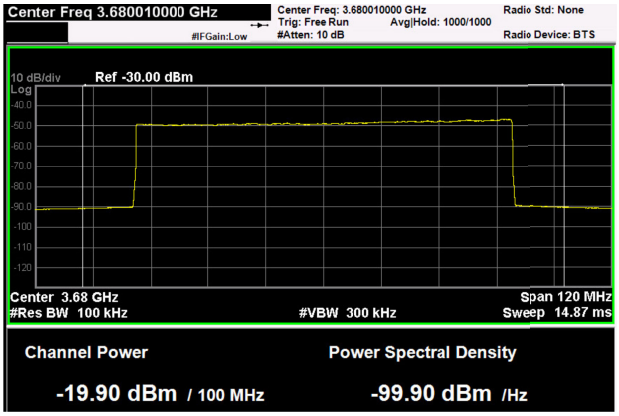

FIGURE 16. Channel power measurement.

V. CRITICAL POINTS AND LIMITATIONS OF THE TECHNIQUE

Measurements showed that the procedure is simple and effective. However, as any measurement techniques, it has some critical points and some limitations. One of the critical points of the technique is that the estimation of F_{beam} requires to force the data beam toward the measurement position. In the above example a customized phone specifically modified to force downloading data using UDP protocol has been used with excellent results. However, in practical applications the use of 'on the shelf' systems available on the market is preferable. This problem has been investigated considering two different solutions.

A first solution is to use a standard 5G phone to force data traffic toward the measurement position. In order to simulate this solution, a phone was used to download a 4K video. The power per RE is shown in Fig. 17. In spite of the relatively large amount of downloaded data, the number of REs per frame is modest and highly concentrated in frequency and time. This is also confirmed by the low number of Resource Blocks transmitted during the measurement session (red line in Fig. 18). In the same figure, the transmitted power is also reported (blue line in Fig. 18), confirming the high energy efficiency of the 5G signaling structure. Coming back to the

FIGURE 17. Power level of the REs in case of 4K video dowload by a single UE; the power is represented in false colors.

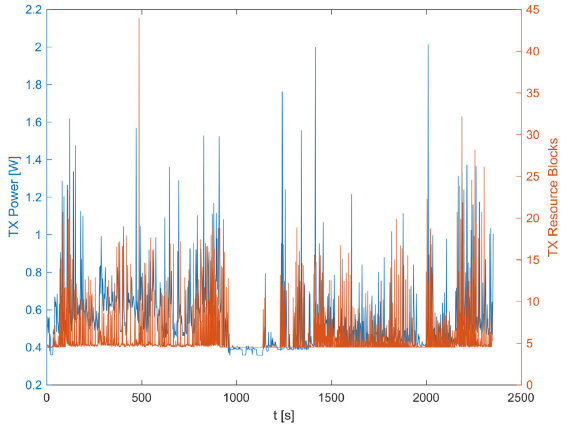

FIGURE 18. Trasmitted power level [dB] and number of transmitted Resource Blocks during the measurement session regarding the 4K video dowloading examples showed in this paper.

measurement of the field amplitude, from our experience, the position of the REs data block in the frequency axis changes with time, and this makes it possible to measure F_{beam} using a zero span measurement in "max hold" provided that the observation time is sufficiently long (Fig. 19). Our experience suggests that a couple of minutes is sufficient.

A different solution involves the use of receivers developed for testing of communication networks, that allows higher flexibility in download parameters. During the test we checked also one of these systems (Rohde & Schwarz Qualipoc Android), successfully imposing a UDP download in the full bandwidth. It is understood that in standard working conditions, i.e. in presence of a large number of users that compete for the network resources, the fraction of the available bandwidth assigned to a single user is not predictable since it is up to the scheduler. However, this second solution seems to be preferable, since it is reasonable to imagine that the scheduler tends to give more bandwidth to the UDP high data-rate receiver, allowing to decrease the measurement time.

As further observation, as noted in Section II, the E_{5G}^{max} gives the maximum field level in an ideal condition in which a single user is connected at the maximum power using all the resources for a continuous time interval that, considering f.i. the ICNIRP guidelines [1], must be not shorter than 6 minutes. In order to compare the result of extrapolation method with channel power measurement, during the research described in this paper we had to reach this specific

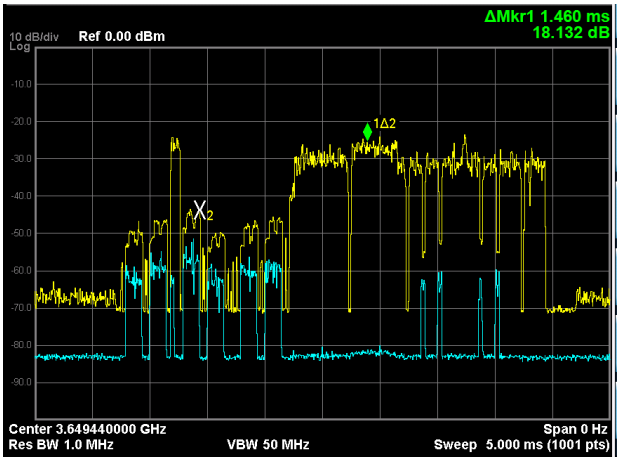

FIGURE 19. Zero span measurement of the signal in 4K video downloading condition (1 MHz RBW); yellow: max-hold trace; blue: average value.

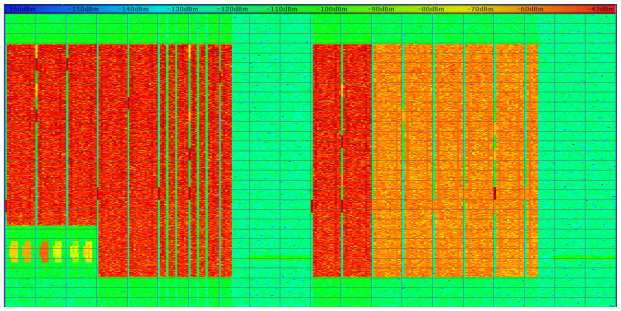

FIGURE 20. The power per RE versus the subcarriers (vertical axis) and the OFDM symbols (horizontal axis) in case of one UE in A and one UE in B and full use of the grid resources; the power level is plotted in false colors.

condition. Indeed, it was extremely hard. Also, in case of UDP and specific software forcing at the highest possible data rate, we were not able to reach the required experimental condition. Indeed, the scheduler did not allow to give all the resources to a single user. In order to reach the full use of the resources, we were forced to use at least two phones placed very close to each other in the measurement position. Furthermore, even in this condition the use of full resources is completely up to the scheduler, and it is not assured for a long time. Our experience suggests that E_{5G}^{max} is a theoretical value that is not reached in any practical condition. For example, Fig. 18 shows the power radiated in a more realistic case (download of a 4K movie), showing a much lower radiated power and use of RBs. Roughly, the actual field level is scaled by the square root of the number of the transmitted RBs compared to the number of total RBs available in the NR carrier bandwidth.

Fig 18 considers a case in which not all the RBs are used. In real applications we must expect that many users compete for the RBs, and all the RBs are consequently used, and dynamically associated to different users. In order to give a more complete picture of the actual field level in 5G systems, we considered a number of case studies observing how the scheduler distributes the power among the users. As an example, we moved one of the UDP UE from point A to the point B shown in Fig 8, forcing again a full use of the resources. It is to be stressed that this is a critical condition since A and B are seen at relatively small angular distance by the transmitting antenna, and consequently the beam toward B radiated a not negligible power density toward A.

The RE grid, reported in Fig. 20, shows that the scheduler splits the available REs between the two users using two directive data beams. The power of REs is drawn in false colors, with red equal to maximum power. The plot clearly shows that in spite of the small angular distance between A and B, the data transmitted to B are received by A at a power level lower than 10 dB compared to the data transmitted to A. As a consequence, loosely speaking, the average power radiated toward the point A is in the order of half the total radiated power, and the field amplitude turns out to be scaled of almost $\sqrt{2}$ compared to E_{5G}^{max}. As noted, this is a critical example. UEs having larger angular distance receive lower power.

According to the above examples we expect that the average amplitude of the field actually received in real conditions is generally significantly lower than E_{5G}^{max}. As noted in Section II, a more realistic field level, i.e. an ''actual'' maximum exposure level, requires to take into account an additional factor (F_{PR}) as indicated by the International Electromechanical Commission (IEC) [2], [3]. Estimation of F_{PR} factor is extremely complex since the exposure of a user depends also on the activity of the other users (see for example the interactive simulation reported in [19]), and is beyond the scope of the paper. More detailed information on F_{PR} factor and on the approaches used for the assessment of the actual maximum exposure can be found in [3], [25].

As further observation, we note that the extrapolation formula does not include the MU-MIMO case. The details of the MU-MIMO implementation depend on the vendors, and the effectiveness of any solution regarding this technology requires experimental test. However, before concluding this Section, some comments on the measurement of EMF level in MU-MIMO are in order.

As discussed in Section II, in MU-MIMO the energy is shared among the UEs, which are sufficiently spatially separated. The maximum number of layers in case of MU-MIMO is 16, while the typical maximum number of layers for current mobile phones is 4, giving a large number of possible scenarios ranging from 16 different UEs using one layer each, to 4 UEs using 4 layers each. As a consequence, in MU-MIMO spatial multiplexing there is a large number of possible distributions of the energy among the UEs located in different positions, and forcing a communication in the measurement point does not assure the possibility to evaluate the maximum EMF level if there are other communication incurred.

Coming back to the electromagnetic analysis of MIMO systems, we can imagine the field as a superposition of basis each having almost the same power. In this model the UE is able to measure the power associated to the fraction of basis field functions whose energy is focused toward it (see fig. 3). Under these assumptions, the maximum power per RE is given by the maximum power per RE evaluated in the measurement point, corrected by a factor given by the ratio between the total number of layers used by 5G system and the number of layers used in the communication with the UE in the measurement point. However, as previously stressed, details of the implementation of MU-MIMO, including the distribution of the power among the UEs, are totally under the decision of the vendors.

As last note, it is useful to stress that the procedure followed in this paper uses some data belonging to the rich set of signals associated to NR transmission, in particular for PBCH-DMRS and SSB power level measurement. The choice of what and how much information is made available by the signaling structure of the NR is an intriguing problem that offers many different solutions for EMF level measurement. For example, in the procedure proposed in [6] the maximum power per RE of the SSB is measured in zero span instead of using data from the NR signal set.

The above example shows how the estimation of the parameters in the extrapolation formula (1) can be obtained using different approaches, i.e. from measurement of the signal in air or from NR signaling data. This observation opens new perspectives in the field level estimation by 5G base stations in case of MU-MIMO. Since MU-MIMO is a technological behavior of 5G that could affect any extrapolation methods based of the traffic power (PDSCH), identification of what data is convenient to measure and what data is convenient to extract for 5G signaling data is an important problem that is currently object of investigation by the authors of this paper.

VI. CONCLUSIONS

In this paper the problem of maximum power extrapolation for assessment of 5G base station exposure is discussed and a technique for estimation of the EMF level is tested. The results confirm the effectiveness of the proposed technique in the case under test, that regards NR signals radiated by a 5G base station using TDD multiplexing and SU-MIMO SDMA technique.

The paper includes an analysis of the NR at the lowest physical level, i.e. at the level of the electromagnetic field radiated by the base station antenna, clarifying the connection among the parameters used at 'network level', f.i. the antenna ports, and the quantity of interest in EMF measurements, i.e. the space-time configuration of the electromagnetic field.

The analysis carried out in this paper makes it clear that the complexity and high flexibility of NR standard represents a formidable challenge for the development of maximum power extrapolation techniques. The large number of details, in particular on the radiating system, that are demanded to the designer of the equipment makes it difficult to develop measurement techniques that are at the same time general and simple.

In particular, the development of extrapolation techniques for general MU-MIMO communication represents a particularly demanding challenge. As noted in Section IV, the procedure followed in this paper takes advantage of some data belonging to the rich set of signals associated to NR transmission. A possible approach is to extend the use of data signaling in the extrapolation procedure. This observation opens new perspectives in the estimation of EMF radiated by 5G base stations, that are currently object of investigation by the authors on this paper.

It must be stressed that the estimation of maximum power is only a part of the problem of field exposure evaluation, as also discussed in this paper. The maximum field level is representative of an ideal and practically unrealistic condition in which a single user is connected at maximum power using all the resources for a continuous time interval. Its value is a ''deterministic'' quantity used as 'reference level' for the estimation of human exposure in realistic conditions using proper F_{PR} scalar factors including statistical conditions. As discussed in the paper, the technique presented in this paper has been tested in SU-MIMO condition. The extension of the technique to MU-MIMO is under development. However, an alternative approach is to consider as 'reference level' the maximum field in the SU-MIMO condition, taking statistically into account the impact of MU-MIMO in an 'extended' version of the F_{PR} factor. The choice of the factors that must be obtained by measurements, and the ones that must be included in the statistical F_{PR} factor is a further degree of freedom that must balance the complexity of field measurements and the accuracy of statistical approaches.

APPENDIX A
INFORMATION CARRIED ON SPATIAL CHANNELS

In order to have a unified model for the many SDMA strategies, let us consider the abstract model of the communication system at the basic physical level proposed in [15], [16]. The transmitter is modeled as a harmonic electromagnetic source placed in the volume D having surface Σ, whereas the receiver is represented by an observer that has access to the electromagnetic field distribution on an observation manifold Ω.

The field E measured on the domain Ω is related to the current distribution J on the source by a linear relationship (i.e. the radiation operator) [17], [23]:

$$E(\mathbf{r}) = \int_D G(\mathbf{r}, \mathbf{r}')\, J(\mathbf{r}') d\mathbf{r}' \tag{5}$$

wherein $\mathbf{r} \in \Omega$, G is the Green's function, i.e. the spatial impulse response. E and J are square integrable functions (standard L_2 norm in Hilbert spaces is considered).

Now let us represent the current distribution function $J(\mathbf{r}')$ as Fourier series using the $\mathbf{v}(\mathbf{r}') = \{v_1(\mathbf{r}'), v_2(\mathbf{r}'), \ldots,$

$v_k(\mathbf{r}'), \ldots\}$ basis:

$$J(\mathbf{r}') = \sum_{k=1}^{\infty} x_k v_k(\mathbf{r}') \tag{6}$$

The vector $\mathbf{x} = \{x_1, x_2, \ldots, x_k, \ldots\}$ that collects all the (infinite) coefficients x_k of the expansion can be represented as a point having coordinate $\{x_1, x_2, \ldots, x_k, \ldots\}$ in an infinite dimensional space. Note that the current has finite energy, i.e. $\|\mathbf{x}\|$ is finite. Without loss of generality we will suppose $\|\mathbf{x}\| < 1$. Consequently, all the current distributions on the source are represented by points belonging to an open hyper-ball X having unit radius placed in an infinite dimensional space [15].

In the same way we can expand the field $E(\mathbf{r})$ on Ω in a series using the $\mathbf{u}(\mathbf{r}) = \{u_1(\mathbf{r}), u_2(\mathbf{r}), \ldots, u_k(\mathbf{r}), \ldots\}$ basis:

$$E(\mathbf{r}) = \sum_{k=1}^{\infty} y_k u_k(\mathbf{r}) \tag{7}$$

The vector $\mathbf{y}$ that collects all the components y_k, $k = 1, 2, \ldots$ is a point in an *infinite* dimensional space.

Due to the linear relationship between currents and fields, the $\mathbf{x}$ and $\mathbf{y}$ vectors are related by a matrix (i.e. the radiation matrix). The matrix can be diagonalized choosing a proper $\mathbf{v}(\mathbf{r}')$ and $\mathbf{u}(\mathbf{r}')$ basis [15] given by Singular Value Decomposition [20], obtaining

$$\mathbf{y} = \mathbf{A}\mathbf{x} \tag{8}$$

wherein

$$\mathbf{A} = \begin{pmatrix} \sigma_1 & 0 & 0 & \ldots \\ 0 & \sigma_2 & 0 & \ldots \\ 0 & 0 & \sigma_3 & \ldots \\ \ldots & \ldots & \ldots & \ldots \end{pmatrix} \tag{9}$$

Accordingly the components of $\mathbf{x}$ and $\mathbf{y}$ vectors are related by the following simple relationship:

$$\begin{aligned} y_1 &= \sigma_1 x_1 \\ y_2 &= \sigma_2 x_2 \\ &\ldots \\ y_k &= \sigma_k x_k \\ &\ldots \end{aligned} \tag{10}$$

The elements σ_k along the main diagonal are called the *singular values* of the matrix $\mathbf{A}$ [20]. They are non negative and we suppose that they are sorted in descending way, i.e. $\sigma_1 \geq \sigma_2 \geq \ldots$,. Furthermore, it is possible to show that $\sigma_k \to 0$ when $k \to \infty$.

Now, let us suppose that the received signal is affected by an ϵ level error caused by the noise and more generally by measurement uncertainties. We have:

$$\begin{aligned} y_1 &= \sigma_1 x_1 + \epsilon \\ y_2 &= \sigma_2 x_2 + \epsilon \\ &\ldots \\ y_k &= \sigma_k x_k + \epsilon \\ &\ldots \end{aligned} \tag{11}$$

A rigorous approach for series approximation is based on the Kolmogorov $n-$width [15], [21]. Intuitively when $\sigma_k < \epsilon$ we have that $\sigma_k x_k$ is covered by ϵ, making it impossible to retrieve x_k from y_k.

Consequently, in presence of an ϵ level of uncertainty the series can be approximated using a finite number of terms. The minimum number of such terms is the ϵ-Number of Degrees of Freedom of the field (NDF_ϵ) [15]. The above analysis has been limited to a scalar field for sake of simplicity. In case of vector field, the NDF_ϵ turns out to be twice the scalar case.

As a consequence, *any* field configuration on the receiving domain *distinguishable at an ϵ level of approximation* can be represented as:

$$E(\mathbf{r}) = \sum_{k=1}^{NDF\epsilon} y_k u_k(\mathbf{r}) \tag{12}$$

In order to clarify the connection between the above expression and information carried on space channels, let us consider the representation of a time domain signal having angular frequency ω:

$$s(t) = a(t)\cos(\omega t) + b(t)\sin(\omega t) \tag{13}$$

We can note a strict similarity with the representation of the field distribution in the space domain. With reference to Eq. 13, the presence the two time-orthogonal basis allows to double the amount of information compared to the case in which we use only one basis, f.i. only sine. The physical counterpart of the two bases functions are the I/Q channels in receiving equipment.

With reference to Eq. 12, we can send independent information by changing the values of the coefficients y_k. Clearly, the amount of information increases with the number of basis function $\{u_k\}$. The more bases we use, the more information can be associated to the electromagnetic field. Skipping to communication, this ability to send information by varying the spatial configuration of the field is at the basis of the MIMO systems.

A detailed discussion of the meaning of the NDF_ϵ and its role in spatial channels is beyond the scope of this paper, and can be found in [15]–[17]. We note only that the NDF_ϵ is the equivalent of the Number of Degrees of Freedom of time-signals (*TNDF*) introduced in the Shannon theory [22]. In Shannon theory, the *TNDF* is given by the time-bandwidth product and fixes a fundamental limitation in the use of the time resource. Analogously, NDF_ϵ is given by the space-spatial bandwidth product [17] and fixes a fundamental limitation for any communication system using the space resource, including the systems based on sophisticated radiating systems proposed not only for 5G but also for the next 6^{th} generation [16], [24]. Indeed, the above theory allows to look at modern antennas from different perspectives. For example, Massive MIMO antennas are basically antennas radiating an electromagnetic field having a huge

value of NDF_ϵ, or, equivalently, they radiate fields having wide (spatial) bandwidth [16], [17].

The above outlined analysis shows also that rigorously it is not possible to define the Gain of MIMO antennas. In fact, the spatial field configuration is used to encode information and the power density distribution in the space changes according to the encoded symbol [17].

APPENDIX B
DESCRIPTION OF THE MAXIMUM POWER EXTRAPOLATION PROCEDURE

This Appendix is devoted to the description of the instrumental setting and procedures adopted for the estimation of the parameters involved in the extrapolation formulas discussed in Section II, and reported in the following for sake of reader convenience, wherein Eq. (2)-(4) have been substituted in Eq. (1):

$$E_{5G}^{max} = AF\sqrt{\frac{N_{sc}F_{TDC}F_{beam}Z_{in} < P_{RE}^{PBCH-DMRS} >}{\alpha R}} \quad (14)$$

A. TOTAL NUMBER OF SUBCARRIERS N_{sc}

The total number of subcarriers N_{sc} is defined as 12 N_{RB}, where N_{RB} represents the total number of Resource Blocks available for the signal. The value of N_{RB} depends on both the signal bandwidth and the subcarrier spacing, and is reported in he Tables 5.3.2-1 and 5.3.2-2 of [10].

B. TIME DUTY CYCLE FACTOR F_{TDC}

The time duty cycle factor F_{TDC} is the fraction of the signal frame reserved for downlink transmission. In the case of no *a priori* knowledge about the specific TDD scheme implemented by the signal under investigation, a direct determination of F_{TDC} can be carried out through a zero span measurement using a scalar spectrum analyzer by means of the following procedure based on zero-span measurement [8]:

- central frequency set to the 5G central carrier;
- RBW as large as allowed by the spectrum analyzer (note that RBW should not be larger than the signal bandwidth, however);
- VBW was set to a value greater than RBW: this setting is not so important for a measurements aimed to determine time intervals, but in general this choice allows to avoid loss of energy contribution in a noise-like signal;
- sweep time set as a multiple of a frame period (10 ms);
- a periodic trigger according to the frame period (100 Hz);
- trace mode set to max-hold, in order to easily distinguish between downlink and uplink slots.

The acquired trace allows for an effective identification of the uplink slots, since the associated received power is several orders of magnitude lower than that related to downlink slots. Experimental evidence suggests an acquisition time of at least 10 sec per trace, in order to ensure the proper rising of downlink slots.

C. PBCH-DMRS AVERAGE POWER PER RESOURCE ELEMENT $< P_{RE}^{PBCH-DMRS} >$

Modern VSAs provide a reliable measurement of PBCH-DMRS power per RE, averaged over the SSBs in a burst, through demodulation analysis of the 5G signal. To ensure a correct demodulation of SSBs and, therefore, the reliability of PBCH-DMRS power measurement, a set of parameters defining the characteristics of the 5G signal under measurement must be provided to the instrument, such as:

- SSB numerology μ;
- SSB frequency offset with respect to the signal center frequency;
- SSB pattern (Case A, B, C, D, E);
- SSB periodicity;
- The maximum number of SSBs allowed for the specific pattern (L_{max});
- TDD scheme.

This implies that the measurement session should be sustained by a preliminary survey aiming at acquiring all the mandatory information about the investigated signal. Some VSAs are equipped with automated detection routines which provide a reliable SSB demodulation, making the PBCH-DMRS power detection a quite easy task.

D. SSB POWER SCALE FACTOR R

The power scale factor R is as the ratio between the average detected power of all the SSBs in a burst and the power of the strongest SSB in the burst [8]. As shown in Fig. 14, the VSA provides the received power for all the SSBs of a burst, allowing for a easy determination of R. Since the procedure relies on a demodulation analysis, the knowledge of all those parameters discussed in the previous section is still required.

Some VSAs provide the detected PBCH-DMRS power for each SSB instead of the averaged value. In this case, the user can directly use the PBCH-DMRS power related to the strongest SSB with no need to compute R factor.

E. BEAMFORMING FACTOR F_{beam}

The beamforming parameter F_{beam} takes into account the effect of a potential boost of the traffic beams with respect to maximum EMF level received from the pilot channel, due to the effect of beamforming produced by the use of mMIMO antennas. To ensure a correct estimate of F_{beam}, the measurement should be carried out in conditions of maximum EMF exposure, i.e. with a traffic beamformed beam pointing towards the receiving antenna. This requirement can be obtained by placing an UE next to the receiving antenna, while exchanging data traffic with the 5G source under investigation.

F_{beam} can be measured with a zero span mode measurement using the following settings:

- center frequency set to the central frequency of the SSB;
- RBW smaller than 127 sub-carriers (e.g. 1 MHz);

- Also in this case, VBW was set to a value greater than RBW, even if the influence of this parameter is quite weak in the evaluation of a ratio between power levels;
- trace mode set to max-hold;
- detector set to peak;
- sweep time set to half-frame (5 ms);
- a periodic trigger according with the frame period (100 Hz);
- a fine-tuned trigger offset to ensure that both SSBs and traffic slots are visible on the acquired trace at the same time.

The ratio between the power of the highest traffic level and the power of the highest SSB represents F_{Beam} factor. Since the power of the highest traffic level is quite variable within a single slot, the power value taken into account was the average of the values of the pixels in the zero span trace in each maximum load slot. It is understood that in the case of different numerologies used for traffic channels and SSB, a proper scaling factor depending on the numerologies must be introduced.

ACKNOWLEDGMENT

The authors would like to thank Dr. Roberto Cosentino (Rohde Schwarz company) and Dr. Massimo Bauco (Rohde Schwarz company) for the useful discussion on the equipment for 5G signal measurement, and Dr. Mattia Vaccarono (Arpa Piemonte) and Dr. Stefano Coltellacci (Arpa Lazio) for their precious help in the measurements.

REFERENCES

[1] *Guidelines for Limiting Exposure to Electromagnetic Fields (100 kHz to 300 GHz)*, document Health Phys 118(00):000-000; ICNIRP, 2020, doi: 10.1097/HP.0000000000001210.
[2] *Determination of RF Field Strength, Power Density and SAR in the Vicinity of Radiocommunication Base Stations for the Purpose of Evaluating Human Exposure*, Standard IEC 62232:2017, 2017.
[3] *Case Studies Supporting IEC 62232—Determination of RF Field Strength, Power Density and SAR in the Vicinity of Radiocommunication Base Stations for the Purpose of Evaluating Human Exposure*, Standard IEC/TR 62669:2019, 2019.
[4] B. Xu, K. Zhao, B. Thors, D. Colombi, O. Lundberg, Z. Ying, and S. He, "Power density measurements at 15 GHz for RF EMF compliance assessments of 5G user equipment," *IEEE Trans. Antennas Propag.*, vol. 65, no. 12, pp. 6584–6595, Dec. 2017.
[5] R. Pawlak, P. Krawiec, and J. Zurek, "On measuring electromagnetic fields in 5G technology," *IEEE Access*, vol. 7, pp. 29826–29835, 2019.
[6] S. Aerts, L. Verloock, M. Van Den Bossche, D. Colombi, L. Martens, C. Tornevik, and W. Joseph, "*In-situ* measurement methodology for the assessment of 5G NR massive MIMO base station exposure at sub-6 GHz frequencies," *IEEE Access*, vol. 7, pp. 184658–184667, 2019.
[7] H. Keller, "On the assessment of human exposure to electromagnetic fields transmitted by 5G NR base stations," *Health Phys.*, vol. 117, no. 5, pp. 541–545, Nov. 2019.
[8] D. Franci, S. Coltellacci, E. Grillo, S. Pavoncello, T. Aureli, R. Cintoli, and M. D. Migliore, "An experimental investigation on the impact of duplexing and beamforming techniques in field measurements of 5G signals," *Electronics*, vol. 9, no. 2, p. 223, Jan. 2020.
[9] D. Franci, S. Coltellacci, E. Grillo, S. Pavoncello, T. Aureli, R. Cintoli, and M. D. Migliore, "Experimental procedure for fifth generation (5G) electromagnetic field (EMF) measurement and maximum power extrapolation for human exposure assessment," *Environments*, vol. 7, no. 3, p. 22, Mar. 2020.
[10] *NR; Base Station (BS) Radio Transmission and Reception (Release 15)*, document 3GPP TS 38.104 V15.5.0, May 2019.
[11] S. Ahmadi, *5G NR: Architecture, Technology, Implementation, and Operation of 3GPP New Radio Standards*. New York, NY, USA: Academic, 2019.
[12] M. Kottkamp, A. Pandey, D. Raddino, A. Roessler, and R. Stuhlfauth, *5G New Radio. Fundamental Procedures and Technical Aspects*. Munchen, Germany: Rhode & Schwarz, 2019.
[13] E. Dahlman, S. Parkvall, and J. Skold, *5G NR: The Next Generation Wireless Access Technology*. New York, NY, USA: Academic, 2018.
[14] T. David and P. Viswanath, *Fundamentals of Wireless Communication*. Cambridge, U.K.: Cambridge Univ. Press, 2005.
[15] M. D. Migliore, "On electromagnetics and information theory," *IEEE Trans. Antennas Propag.*, vol. 56, no. 10, pp. 3188–3200, Oct. 2008.
[16] M. D. Migliore, "Horse (electromagnetics) is more important than horseman (information) for wireless transmission," *IEEE Trans. Antennas Propag.*, vol. 67, no. 4, pp. 2046–2055, Apr. 2019.
[17] M. D. Migliore, "On the role of the number of degrees of freedom of the field in MIMO channels," *IEEE Trans. Antennas Propag.*, vol. 54, no. 2, pp. 620–628, Feb. 2006.
[18] M. D. Migliore, "Some Notes on the Verification of the Exposure Limits in 5G Systems," in *Proc. IEEE Int. Symp. Meas. Netw. (M&N)*, Jul. 2019, pp. 1–5.
[19] *5G Antennas in a Nutshell*. Accessed: May 13, 2020. [Online]. Available: https://sites.google.com/unicas.it/electromagnetic-information/home
[20] G. Golub, C. Van Loan, *Matrix Computation*. London, U.K.: The Johns Hopkins Univ. Press, 1996.
[21] A. Pinkus, *n-Widths in Approximation Theory*. Berlin, Germany: Springer-Verlag, 1985.
[22] A. D. Wyner, "The capacity of the band-limited Gaussian channel," *Bell Syst. Tech. J.*, vol. 45, no. 3, pp. 359–395, Mar. 1966.
[23] G. W. Hanson and A. B. Yakovlev, *Operator Theory in Electromagnetics: An Introduction*. New York, NY, USA: Springer-Verlag, 2002.
[24] A. Pizzo, T. L. Marzetta, and L. Sanguinetti, "Degrees of freedom of holographic MIMO channels," 2019, *arXiv:1911.07516*. [Online]. Available: http://arxiv.org/abs/1911.07516
[25] B. Thors, A. Furuskär, D. Colombi, and C. Törnevik, "Time-averaged realistic maximum power levels for the assessment of radio frequency exposure for 5G radio base stations using massive MIMO," *IEEE Access*, vol. 5, pp. 19711–19719, 2017.

SARA ADDA received the M.Sc. degree *(cum laude)* in physics and the master's degree in health physics from Turin University, Italy, in 1998 and 2003, respectively.

She worked for one year, from 1998 to 1999, at ENEA Casaccia, Rome, within the Interdepartmental Computing and High Performance Networks Project, implementing a system for the simulation of electromagnetic field dynamics in complex environments through the use of massively parallel architectures. Since 1999, she has been working with the Physical and Technological Risk Department, ARPA Piedmont, dealing with the control and monitoring of non-ionizing radiation and the development of theoretical forecasting/numerical calculation methods, both in the low and high-frequency ranges. She is involved in the activities with the Italian Electrotechnical Committee (CEI) working groups, for the drafting of technical standards on measurement and evaluation methods for human EMF exposure, and she deals with the theoretical and practical aspects related to the measurement of electromagnetic fields in the workplace. In this context, she is the Representative of the Piedmont Region with the Interregional Technical Coordination Group. She participates in European (twinning Italy–Poland project) and international collaborative projects (Arpa Piemonte–Beijing Municipal Environmental Protection Bureau) on methods and techniques for measuring and evaluating human exposure to EMF both in the workplace and in the living environment.

TOMMASO AURELI received the M.Sc. degree in biological science from the Sapienza University of Rome, Rome, Italy, in 1985. He joined Agenzia per la Protezione Ambientale del Lazio (ARPA Lazio), in 2002. From 2004 to 2018, he was the Director of the EMF Division, being involved in both measurement and provisional evaluation EMF from civil sources. He is currently the Director of the Department of Rome.

STEFANO D'ELIA received the M.Sc. degree *(cum laude)* in electronics engineering from the Sapienza University of Rome. He joined Vodafone Italia S.p.A (formerly Omnitel Pronto Italia), in 1998. In 2002, he was appointed as a Convenor of the Working Group Mobile Base Stations with the Technical Committee 106 of the Italian Electro Technical Committee (CEI), acting as a national delegate of several standardization bodies on EMF measurements and calculations. In 2012, he was appointed as a Vodafone Distinguished Engineer, one of the highest steps in the technical career path at Vodafone Italia S.p.A, where he is currently covering the role of the Mobile Access Integrated Solutions Manager of Group Networks.

DANIELE FRANCI received the M.Sc. degree *(cum laude)* and the Ph.D. degree in nuclear and subnuclear physics from the Sapienza University of Rome, Rome, Italy, in 2007 and 2011, respectively. From 2009 to 2011, he was a Technology Analyst with Nucleco S.p.A, involved in the radiological characterization of radioactive wastes from the decommissioning of former Italian nuclear power plants. He joined Agenzia per la Protezione Ambientale del Lazio (ARPA Lazio), in 2011, being involved in RF-EMF human exposure assessment. Since 2017, he has been involved in the activities with the Italian Electro Technical Committee (CEI) for the definition of technical procedures for EMF measurement from 4G/5G mMIMO sources.

ENRICO GRILLO received the M.Sc. degree in electronics engineering from the Seconda Università di Napoli, Aversa, Italy, in 1999.

In 2000, he works on RF to grow up the first 3G telecommunication radio network. Since 2005, he has been involved as a Research Technician in the prevention and monitoring of electromagnetic pollution with Agenzia per la Protezione Ambientale del Lazio (ARPA Lazio), the local environmental agency of the Lazio Region.

MARCO DONALD MIGLIORE (Senior Member, IEEE) received the Laurea degree (Hons.) and the Ph.D. degree in electronics engineering from the University of Naples, Naples, Italy.

He was a Visiting Professor with the University of California San Diego, San Diego, La Jolla, CA, USA, from 2007 to 2008 and in 2017, the University of Rennes I, Rennes, France, in 2014 and 2016, the Centria Research Center, Ylivienka, Finland, in 2017, the University of Brasilia, Brazil, in 2018, and Harbin Technical University, China, in 2019. He is a Full Professor with the University of Cassino and Southern Lazio, Cassino, Italy, where he is also the Head of the Microwave Laboratory and the Director of studies of the ITC courses. His current research interests include the connections between electromagnetism and information theory, the analysis, synthesis, and characterization of antennas in complex environments, antennas and propagation for 5G, ad hoc wireless networks, compressed sensing as applied to electromagnetic problems, and energetic applications of microwaves. He was a Speaker of the Summer Research Lecture Series of the UCSD CALIT2 Advanced Network Science, in 2008. He is a member of the ELEDIA@UniCAS Research Laboratory, the National Interuniversity Research Center on the Interactions Between Electromagnetic Fields and Biosystems (ICEMmB), where he is the Leader of the 5G Group, the Italian Electromagnetic Society (SIEM), and the National Interuniversity Consortium for Telecommunication (CNIT). He serves as a referee for many scientific journals and has served as an Associate Editor for the IEEE TRANSACTIONS ON ANTENNAS AND PROPAGATION.

SETTIMIO PAVONCELLO was born in Rome, Italy, in 1973. He received the M.Sc. degree in telecommunication engineering from the Sapienza University of Rome, Rome, in 2001.

Since 2002, he has been working with the EMF Department, Agenzia per la Protezione Ambientale del Lazio (ARPA Lazio), Rome. He is specialized in electromagnetic field measurements and EMF projects evaluation related to radios, TVs, and mobile communications systems maturing huge experience in the use of broadband and selective instruments. In past years, he has deepened in the issues related to measurements on LTE and NB-IoT signals. Since 2018, he has been actively involved in the working group of the Italian Electrotechnical Committee aimed at defining measurement procedures for mobile communications signals and is currently engaged in various projects concerning measurement on 5G signals.

FULVIO SCHETTINO received the Laurea degree (Hons.) and the Ph.D. degree in electronics engineering from the University of Naples, Naples, Italy. He is currently an Associate Professor with the University of Cassino and Southern Lazio, Cassino, Italy. He is a member of the ELEDIA@UniCAS Research Laboratory, the National Interuniversity Research Center on the Interactions Between Electromagnetic Fields and Biosystems (ICEMmB), the Italian Electromagnetic Society (SIEM), and the National Interuniversity Consortium for Telecommunication (CNIT). His current research interests include numerical electromagnetics, regularization methods, the connections between electromagnetism and information theory, the analysis, synthesis, and characterization of antennas in complex environments, antennas and propagation for 5G, and the energetic applications of microwaves.

RICCARDO SUMAN was born in Ivrea, Italy, in 1974. He received the B.Sc. degree in telecommunication engineering from the Politecnico di Torino, Italy, in 1996. Since 1996, he has been with Vodafone Italia S.p.A, Italy, (formerly Omnitel Pronto Italia), where is currently working as an Antenna Matter Expert. He also participates in the recommendation on base station active antenna standards (BASTA AA) by NGMN Alliance. Since 2012, he has been involved in activities related to EMF focusing on measuring and modeling electromagnetic fields and electromagnetic exposure assessment of base stations for mobile communications. He is involved in the activities with the Technical Committee 106 of the Italian Electro Technical Committee (CEI) and a National Delegate of the IEC TC106.